2020 IEEE/RSJ International Conference on Intelligent Robots and Systems (IROS)
October 25-29, 2020, Las Vegas, NV, USA (Virtual)

# Development of a Maneuverable Un-Tethered Multi-fin Soft Robot

T.V. Truong[1], R.C. Mysa[1], T. Stalin[2], P.M. Aby Raj[3], and P. Valdivia y Alvarado[1,2,3,†]

*Abstract*— **In this paper, the design, fabrication, numerical studies, and preliminary characterization of a multi-fin soft robot are presented. The design is simple, robust, and fully autonomous. The robot has a $216mm$ body length and displays great potential to achieve uncoupled surge (forwards and backwards), sway, and heave motions. Computational fluid dynamic (CFD) studies are employed to evaluate appropriate fin control approaches and their influence on force generation. By using asymmetric input functions to actuate all fins in phase, the robot can achieve close to pure heave motions while single fin symmetric actuation enables forwards, backwards, and sway motions.**

## I. INTRODUCTION

In nature, maneuvering capabilities are essential for negotiating obstacles in complex spatial environments, catching prey, escaping predators, and for ritualistic displays (e.g. mating) [1]. Biologists and engineers have devoted much attention to understand how fish modulate fin motions to correct perturbations and maneuver in complex environments [1][2]. Maneuvering motions include small angular turns that either correct perturbations to some desired heading or reorient fish in a new heading [1][2]. Despite all the work in this area, the development of underwater robots capable of exhibiting similar maneuvering capabilities remains a challenge.

Advances in actuation and materials use have helped innovate various mechanisms for robotic applications. Recently, studies in soft robotics for underwater locomotion have yielded interesting bio-inspired research vehicles including a knife fish [3] and batoids [4][5][6] where the common denominator is the use of a single or two soft flexible fins for locomotion and maneuvering. Frame et al developed a free-swimming soft robotic jellyfish actuated by eight pneumatic tentacle actuators [7], which could execute ascending and sway motions. Partially actuated fins drove the robot sideways motions, but only small speeds were achieved. The unactuated fins contributed to the drag limiting robot speeds. Christianson et al used dielectric elastomer actuators (DEAs) as artificial muscles for a soft jellyfish-inspired robot which was able to swim at ascending speeds of 0.02 Body lengths per second (BL/s) with a portable power supply of 0.25W [8]. Ren et al developed an jellyfish-inspired soft milli-robot actuated by an external oscillating magnetic field [9].

*This project was supported by SUTD's Digital Manufacturing and Design Centre (DManD)

[1]SUTD International Design Centre (IDC)
[2]SUTD Digital Manufacturing and Design Centre (DManD)
[3]Engineering Product Development Pillar, Singapore University of Technology and Design (SUTD)
[†] Corresponding author: pablov@sutd.edu.sg

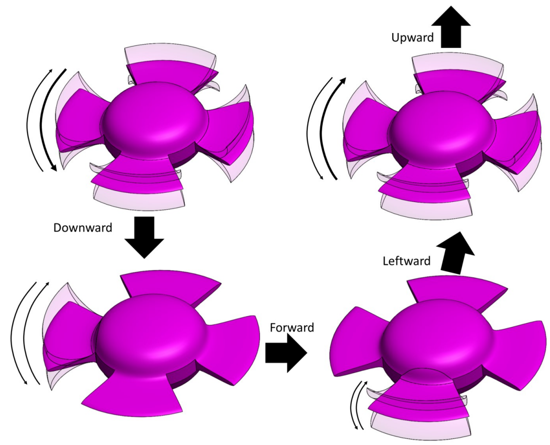


Fig. 1. Illustration of the relationship between the robot fin motions and resulting maneuvers.

The robot could realize multiple functionalities in moderate Reynolds numbers by producing controlled flows around its body using its magnetic composite elastomer lappets. Yu et al reported a jellyfish-inspired swimming robot capable of executing horizontal and ascending maneuvers [10]. They employed four six-bar linkage mechanisms centrally symmetric to drive and regulate the phases of contraction and relaxation of a bell-shaped body. Current underwater soft robots cannot execute uncoupled descending motions. Furthermore, jellyfish-inspired robots with complicated fin actuation designs display limited sway speeds.

Various groups have developed underwater robots with multiple fins for better maneuvering. Berlinger et al. designed a fish robot with four flapping fins driven by magnet-in-coil actuators [11]. Forward swimming was executed using a caudal fin, and yaw turns were implemented using two pectoral fins. Descending motions used flapping motions of a dorsal fin while slow ascending motions used positive buoyancy. Hou et al. studied a fish robot with three fins actuated by Ionic polymer-metal composites (IPMC)[12]. A caudal fin generated propulsive thrust and two pectoral fins enabled turning motions. These and similar bio-inspired robots using caudal, dorsal, and pectoral fins for propulsion can not execute backwards motions, and the ascending motions are not active or require coupling with forward motions to generate the required lift.

To address these drawbacks, the robot design proposed herein uses four independently actuated radial soft fins to achieve uncoupled ascending, descending, forward, backward, and sway motions. The multi-fin design enables fine control of the required robot motions. Heaving motions are

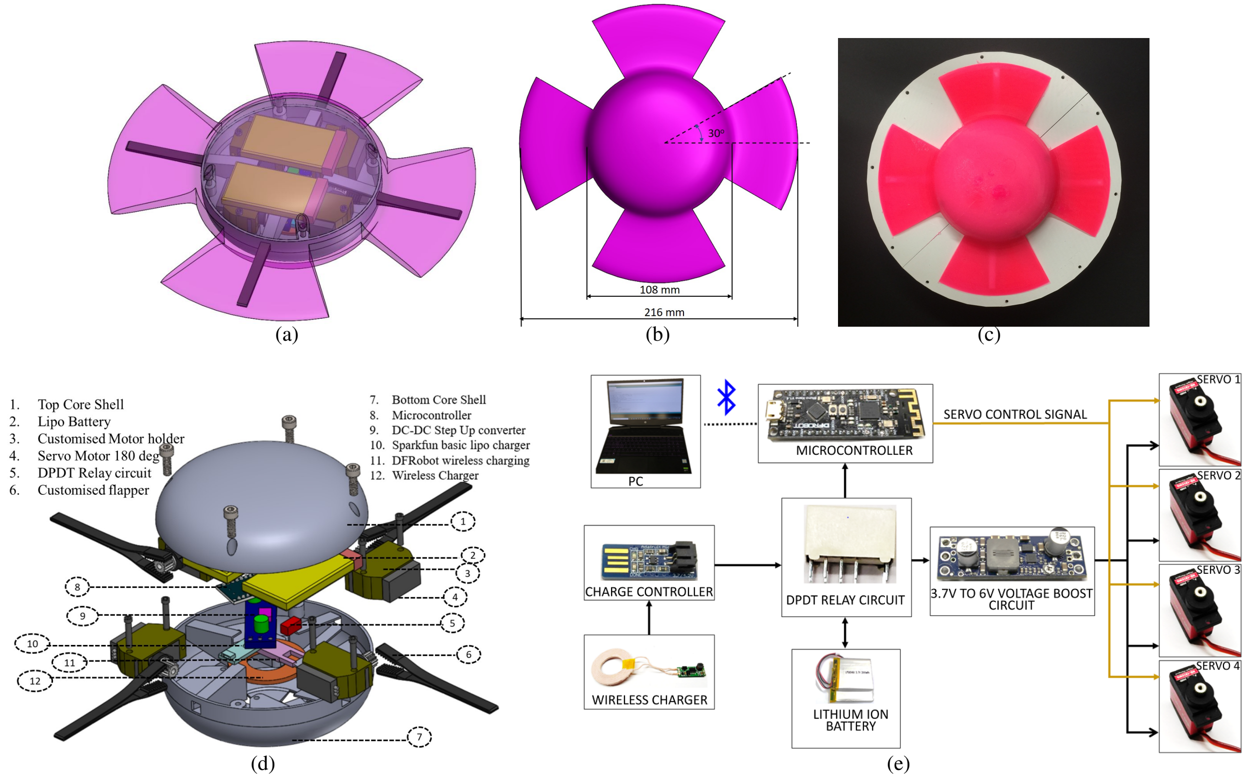


Fig. 2. Robot design: (a) Isometric view of the robot assembly with soft skin encapsulating the 3D printed shell. (b) Top view of the robot showing details of the fin geometry. (c) Top view of mold arrangement for encapsulation (only bottom two halves of the mold are shown for clarity). (d) Exploded view of robot assembly. (e) Block diagram of the robot's electronics architecture.

achieved by synchronized asymmetric fin motions while surge and sway movements can be controlled using single fin actuation.

The paper is organized as follows: the robot design and fabrication are presented in Section II, Section III describes the numerical studies, and the robot maneuvering performance is presented in Section IV. Conclusions and suggested future work are presented in Section V.

## II. DESIGN AND FABRICATION

### A. Design considerations

The robot is driven by 4 independently actuated soft fins located radially around a rigid oblate spheroid body as shown in Fig.1. Maneuverability is achieved through various coordinated fin motions. Heaving motions are achieved by simultaneously flapping all 4 fins with a bias in speeds and amplitudes of upstrokes and downstrokes (e.g. ascending motions have flapping amplitudes biased towards the downstroke cycles with faster speeds on the downstrokes and slower speeds in the upstrokes). Surge and sway motions are achieved by flapping a single fin, the resulting motions are in the directions opposite to the active fin.

The robot design approach follows our previous studies in which a soft silicone polymer is used for the soft body. A platinum cure silicone mix is used to create a continuum between the robot flexible fins and the central body by encapsulating a central shell were actuation, power, and a micro-controller unit are housed. All delicate components are fully encapsulated by the silicone body as shown in Fig.2. A flexible flapper is embedded inside each fin and each flapper mechanism is driven by a servo motor and a rack-pinion mechanism. The robot has a body length (i.e. diameter) of 216 $mm$ and weighs 624 $g$. Fig.2(a) shows details of the robot mechanism design and its main electronic components. The fin span angle (shown in Fig.2(b)) was chosen to be 30 $deg$ following studies indicating the optimality of this value for fish caudal fins [13].

The robot core shell and flappers are 3D printed in ABS using a Fortus 450mc 3D printer. A four part mold is used for encapsulation of the robot shell with a soft silicone skin (Fig.2(c)). The robot is designed to be neutrally buoyant.

### B. Electronics

The robot uses four servo motors (Pololu HD1810 MG) to drive the flapper rack and pinion mechanisms. A central program generates PWM signals based on wave functions to control the servo motors and generate the necessary lift and thrust forces for maneuvering motions. The robot is powered by two flat rechargeable Li-Po batteries (3.7v 2200mAh) connected in parallel. The batteries supply 3.7 volts and a boost converter (Pololu adjustable type) is used to increase the voltage to 6 volts. The main control board is an Arduino Bluno Nano (DFrobot, China), which allows wireless programming. The batteries encapsulated inside the robot's body can be recharged using a wireless charging

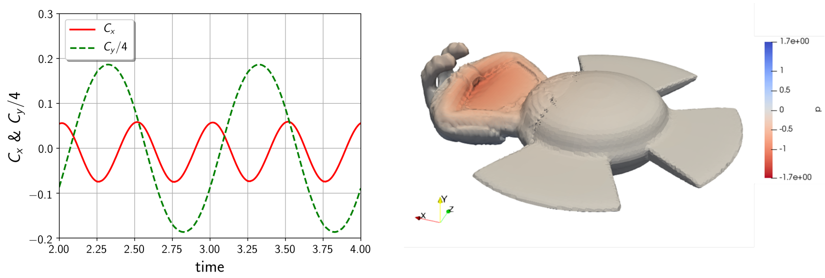


(a) (b)

Fig. 3. Simulation results for single fin force generation: (a) Temporal response of force coefficients $C_x$, $C_y$. (b) Vorticity flow contours colored by pressure at $f = 1Hz$, tip amplitude = $0.06D$, $Re = 188$. The limits for the color legend are $-1.7$ and $1.7$.

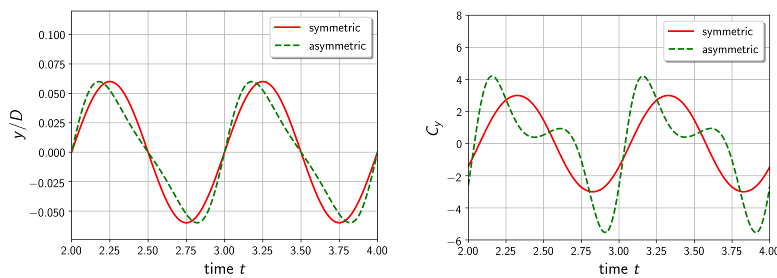


(a) (b)

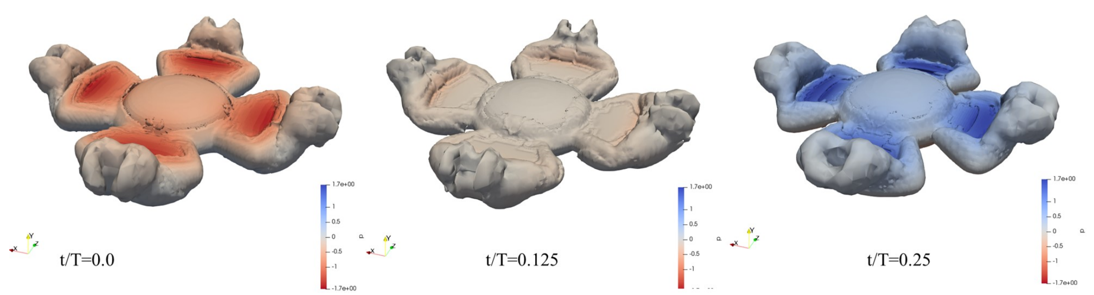


(c)

Fig. 4. Simulation results for multi-fin force generation (frequency = 1, tip amplitude $y_{tip,A} = 0.06D$, Re = 188): (a) Temporal variation of transverse displacement at the tip of the fin. Symmetric wave: $\sin(\Omega t)$; asymmetric periodic wave: $7/16{*}\sin(\Omega t){+}7/64{*}\sin(\Omega t){+}7/128{*}\sin(\Omega t){+}1/512{*}\sin(\Omega t)$. (b) Comparison of force in transverse direction for the given symmetric and asymmetric waves. (c) Vorticity flow contours colored by pressure over the quarter cycle pitching symmetrically. The limits for the color legend are $-1.7$ and $1.7$.

(5V, 5W type) circuit. A transmitter charging coil is fixed to an external charging pod (not shown here) and the receiver charging coil is placed inside the robot close to the ventral surface (see Fig.2(d)). As shown in the system block diagram (Fig.2(e)), all system components are connected to a two coil latched signal relay (Omron GCSK-2) based changeover circuit. The robot has two states: charging mode and ON (i.e. operational) mode. The robot is switched to the ON mode using a magnetic reed switch which connects the battery power to the micro-controller and boosts converter boards. When the robot is placed on its charging pod, the relay latches to charging mode, cutting off power to all other components and connecting the battery to the charging circuit for recharging. The Li-Po charge controller (Adafruit, USA) transfers rated power to recharge and automatically shuts off when an optimum charge is reached. When the batteries are fully charged, the robot is able to operate in water for 33 minutes continuously at the flapping frequency of 1 Hz.

### C. Soft Body Fabrication

Platinum cure silicones (Ecoflex 00-30) and silicone pigments (Silc Pig) were procured from Smooth-on Inc., and carefully pre-mixed before casting. The cast material mixture was prepared by combining the constituents in proper ratios and mixing at 2000 RPM in an ARE-310 Thinky mixer for 2 min, followed by de-foaming at 2200 RPM for 1 min. The mixing ratios are 1 part Ecoflex 00-30 Part A and 1 part Ecoflex 00-30 Part B. In addition, $0.2wt\%$, of pink pigment was added. The mixture was immediately poured into the molds to encapsulate the core-shell and flappers. After 24 hours of curing at room temperature, the robot was carefully removed from the molds (see Fig.2(c)).

## III. NUMERICAL MODEL

Simulations of the soft fin fluid dynamics were used to better understand the robot locomotion capabilities. Fluid flow over an oscillating pitching flexible fin is governed by the incompressible Navier-Stokes equations which are given by,

$$\nabla.\bar{u} = 0, \tag{1}$$

$$\frac{\partial \bar{u}}{\partial t} + \bar{u}.\nabla\bar{u} = -\frac{1}{\rho}\nabla p + \nu\nabla^2\bar{u}. \tag{2}$$

where, $\bar{u}$ is the velocity vector field, $p$ is the scalar pressure, $\rho$ is the fluid density and $\nu$ is the kinematic viscosity of the fluid. For this study, the unsteady incompressible Navier-Stokes equations are solved on a moving grid in an arbitrary Langrangian-Eulerian (ALE) framework using the PIMPLE algorithm implemented in the open source code OpenFOAM.

The PIMPLE algorithm combines a Semi-Implicit Method for Pressure-Linked Equations (SIMPLE) [14] and a Pressure Implicit Splitting of Operators (PISO) [15] for pressure-velocity coupling in incompressible viscous flows. The pressure and velocity are solved using pressure geometric algebraic multi-grid (GMAG) and preconditioned bi-conjugate gradient (PBiCG) respectively. The typical diagonal incomplete LU decomposition is employed as a preconditioner in PBiCG. Detailed information about the mathematical formulations of the solver is given in [16]. The convergence criteria is set to $10^{-6}$ for both pressure and velocity.

The force coefficient for a fin in the $x$-direction (along the fin axis), $C_x$, is defined as:

$$C_x = \frac{1}{\frac{1}{2}\rho_f U^2 S}\int_S \Bigg(\Bigg(-pI + \mu\Bigg(\nabla\bar{u} + (\nabla\bar{u})^T\Bigg)\Bigg)\cdot\mathbf{n}\Bigg)\cdot\mathbf{nx}ds, \tag{3}$$

where $S$ is the surface area of the fin, $U$ is the maximum velocity of the fin, $\mu$ is the dynamic viscosity of the fluid, $\mathbf{n}$ is the unit normal on the surface, $\mathbf{nx}$ is the effective unit normal in $x$ direction.

The force coefficient for a fin in the $y$-direction (normal to the fin planform), $C_y$, is defined as:

$$C_y = \frac{1}{\frac{1}{2}\rho_f U^2 S}\int_S \Bigg(\Bigg(-pI + \mu\Bigg(\nabla\bar{u} + (\nabla\bar{u})^T\Bigg)\Bigg)\cdot\mathbf{n}\Bigg)\cdot\mathbf{ny}ds, \tag{4}$$

where $\mathbf{ny}$ denotes the effective unit normal in the transverse direction $y$. A detailed validation is done in the references [17][18].

## IV. RESULTS

### A. Numerical Studies

Figure 3(a) shows the temporal variations of inline ($x$-direction) and transverse ($y$-direction) force coefficients for a symmetrically pitching single fin at a frequency $f = 1Hz$ with a tip amplitude of $y_{tip,A} = 0.06D$ (where $D$ is the robot diameter) in a still fluid. The Reynolds number based on the maximum fin tip velocity is $Re = 188$. The transverse force is significantly larger than the inline force. The transverse force is symmetric leading to zero mean displacement in the transverse direction. In contrast, the inline force is asymmetric leading to a net thrust generation. As a result, and not surprisingly, a single fin can be used to generate in-line propulsive thrust for forward, backward, and sway maneuvers. The flow contours of vorticity magnitude on the pitching fin, colored by pressure, are shown in Fig.3(b).

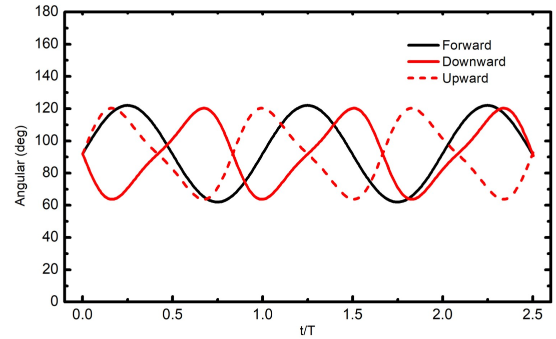


Fig. 5. Fin flapping servo motor control signals: forward, backward, and sway motions use simple harmonic (symmetric) sine waves, ascending motion use asymmetric periodic Fourier sine series, descending motion use inverted asymmetric periodic Fourier sine series.

Numerical studies involving all four fins were also conducted to observe the evolution of the transverse ($y$-direction) force. Figure 4(a) shows the motion of the fin tip for symmetric and asymmetric periodic control signals. For the symmetric periodic flapping signal a simple harmonic sine function was used, whereas a Fourier sine series was used for the asymmetric periodic signal. As a result, the fin motions are slower in the upstroke and faster in the downstroke. The corresponding temporal variations of the transverse force coefficient $C_y$ for symmetric and asymmetric motion are shown in Figure 4(b). The transverse force due to the pitching motions of all four fins is symmetric for the symmetric pitching inputs. For the asymmetric pitching input motions, the faster half cycle results in large transverse force than the slower half cycle, which results in a non-zero average transverse force leading to heave motions. The vorticity contours coloured by pressure over a quarter cycle for symmetrically pitching frequency of 1Hz, $Re = 188$ and pitching amplitude of $0.06D$ are shown in Figure 4(c). The wake is towards the center of the trailing edge of the pitching fin, indicating the contribution is dominated by the added mass effect [19] [20].

### B. Robot manoeuvrability control

Robot control programs were uploaded to the on-board Arduino computer through a Bluetooth connection. The control programs generate control signals based on desired fin flapping frequency, $f$, and flapping amplitude, $A$. The corresponding servo motors input angles $\Phi(t)$ are wave signals, as shown in Fig.5, constructed using simple harmonic

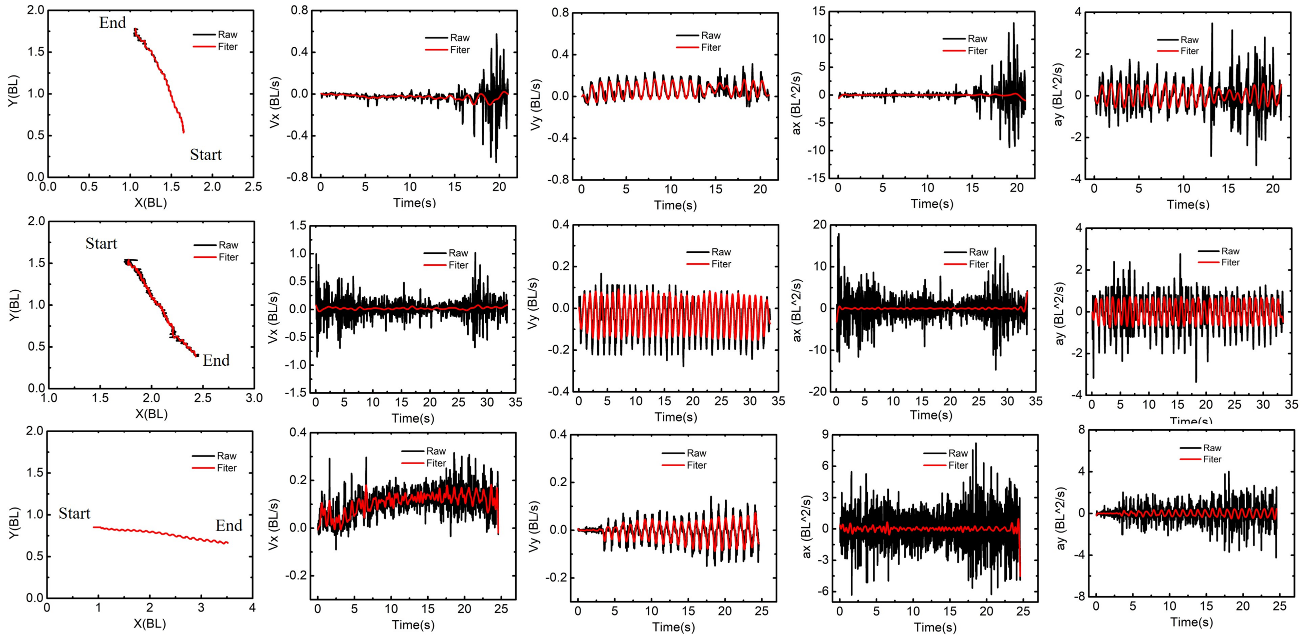


Fig. 6. Kinematic study of the multi-fin robot's motion with first row plots for ascending, second row plots for descending and third row plots for forward motions. The plots in each column are arranged in a sequential order as follows: $x$-trajectory vs $y$-trajectory, $x$-Velocity vs Time, $y$-Velocity vs Time, $x$-Acceleration vs Time, $y$-Acceleration vs Time.

sine waves,

$$\Phi(t) = Initial_{pos} + \frac{A}{2} sin(2\pi f t + \frac{\pi}{2}) + Offset_{pos}, \quad (5)$$

or asymmetric-periodic fourier sine series,

$$\Phi(t) = Initial_{pos} + \frac{7A}{16} * \sin(2\pi f t) + \frac{7A}{64} * \sin(2\pi f t) + \frac{7A}{128} * \sin(2\pi f t) + \frac{A}{512} * \sin(2\pi f t) + Offset_{pos}, \quad (6)$$

or inverted asymmetric-periodic fourier sine series,

$$\Phi(t) = Initial_{pos} - \frac{7A}{16} * \sin(2\pi f t) - \frac{7A}{64} * \sin(2\pi f t) - \frac{7A}{128} * \sin(2\pi f t) - \frac{A}{512} * \sin(2\pi f t) + Offset_{pos}. \quad (7)$$

Where $A$ is the angular displacement of a servo motor (in degrees) and $f$ is the frequency of flapping (in hertz). All experiments were conducted with flapping frequencies of $1Hz$ at 60 degree servo amplitudes using the corresponding servo control signal. The Initial and Offset angles ($Initial_{pos}$ and $Offset_{pos}$) are set to be 100 and 0 degrees respectively.

When only one fin was actuated using a simple harmonic sine wave based on Eqn.5 as a servo control signal, the fin motions displayed equal time periods for upstroke and downstroke cycles, thereby producing a net thrust force to propel the robot in a direction aligned with the fin central axis. When all four fins were actuated using the asymmetric periodic Fourier sine series based on Eqn.6 as a servo control signal, the fin flapping motions were slower on their upstrokes and faster on their downstrokes. The combined effect resulted in a net lift force making the robot swim upwards. When the inverted asymmetric periodic Fourier sine series based on Eqn.7 was used to drive all four fins, the fin flapping motions were faster on their upstrokes and slower on their downstrokes producing a negative lift which made the robot swim downwards.

### C. Free Swimming experiments

Free swimming experiments were conducted in a $120cm$ long, $120cm$ wide, and $70cm$ deep tempered glass tank. Steel rulers were fixed along the tank length and height, and the motions of the robot were recorded using a Nikon Z7 camera. The recorded images were analyzed using Tracker (Open source image analysis tool). Markers painted on the robot fins were tracked to determine displacement trajectories, velocities, and accelerations during programmed movements. Figure 6 shows the kinematics of the various programmed movements. From the kinematic plots it can be observed that the $x$-velocity (forward velocity) for heaving (both ascending and descending) motions is small, almost negligible, and fairly steady. In contrast, for forward motions the $x$-velocity is fairly unsteady but settles into an average value within a short period. The $y$-velocity is unsteady for ascending and descending motion. The trajectory of the robot is not affected much in surging motions as residual $y$-velocities only lead to small deviations, whereas ascending and descending motions have more noticeable deviations due to unbalanced forces. The robot $x$-accelerations during surging motions are negligible while $y$-accelerations show a more marked oscillatory behaviour, likely due to the added mass effects during fin pitching.

Figure 7 shows image sequences of the robot during free swimming experiments. The robot is slightly positively buoyant and it requires more negative thrust to move down.

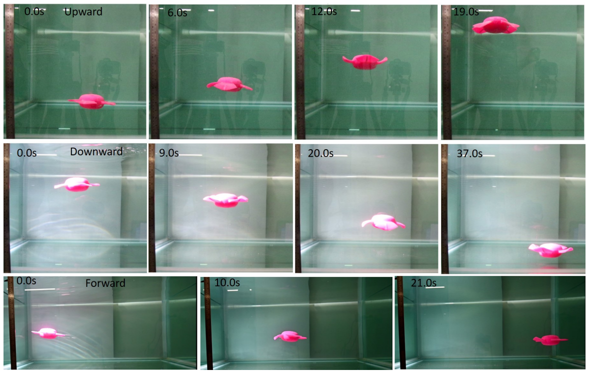


Fig. 7. Robot free swimming experiments: first row of images show ascending motion, second row images show descending motion, and third row of images display forward motion.

Therefore, the robot descends $0.6$ times slower than it ascends. The robot achieves an ascending speed of $0.065BL/s$, a descending speed of $0.04BL/s$, and surging and sway speeds of $0.07BL/s$ at a flapping frequency of $1Hz$.

## V. CONCLUSIONS

This study presents the design, fabrication, and preliminary control tests of a soft un-tethered multi-fin robot. The robot is able to perform heave, forward, backward, and sway motions. Numerical studies were employed to evaluate the propulsive properties of the design and to help determine appropriate fin flapping kinematics. Multi-direction control can be programmed using independent actuation of the four fins. The robot design and control approach can enable complex maneuvers by combining the various fin controllable degrees of freedom.

Numerical studies and free swimming experiments confirmed that a single fin can be used to generate propulsive thrust by employing a simple periodic harmonic sine motion. Whereas four fins employing asymmetric periodic motions using Fourier sine series can be used to propel the robot in heaving motions. For the asymmetric fin pitching motions, faster half cycles result in larger transverse forces compared to slower half cycles. This asymmetry is in turn used to control the direction of heaving motions. In addition, free swimming experiments were employed to characterize the performance of the prototype developed for this study. The robot presented can swim at ascending speeds of $0.065BL/s$, descending speeds of $0.04BL/s$, and at surging and sway speeds of $0.07BL/s$ at a flapping frequency of 1 Hz.

Robot control was not fully optimized and there are many variables that can be explored to further tailor locomotion capabilities. Future work will focus on improving the swimming performance of the robot testing a wider range of flapping frequencies. In addition, alternative flapping control approaches will be explored along with different navigation algorithms and closed loop control. The robot fin configuration and propulsive fluid mechanics are promising to achieve fully uncoupled heave, forward, backward, and sway motions. Furthermore, rugged versions of the platform can offer enough functionality to operate in a wide range of missions in marine environments for civilian and defense applications.

## REFERENCES

[1] J. A. Walker, "Kinematics and performance of maneuvering control surfaces in teleost fishes," *IEEE Journal of Oceanic Engineering*, vol. 29, no. 3, pp. 572–584, 2004.

[2] R. Salazar, A. Campos, V. Fuentes, and A. Abdelkefi, "A review on the modeling, materials, and actuators of aquatic unmanned vehicles," *Ocean Engineering*, vol. 172, pp. 257–285, 2019.

[3] H. Liu, B. Taylor, and O. M. Curet, "Fin ray stiffness and fin morphology control ribbon-fin-based propulsion," *Soft robotics*, vol. 4, no. 2, pp. 103–116, 2017.

[4] P. V. y Alvarado, S. Chin, W. Larson, A. Mazumdar, and K. Youcef-Toumi, "A soft body under-actuated approach to multi degree of freedom biomimetic robots: A stingray example," in *Biomedical Robotics and Biomechatronics (BioRob), 2010 3rd IEEE RAS and EMBS International Conference on*, pp. 473–478, IEEE, 2010.

[5] P. V. y Alvarado, "Hydrodynamic performance of a soft body under-actuated batoid robot," in *Robotics and Biomimetics (ROBIO), 2011 IEEE International Conference on*, pp. 1712–1717, IEEE, 2011.

[6] T. Truong, V. Viswanathan, V. Joseph, and P. V. y Alvarado, "Design and characterization of a fully autonomous under-actuated soft batoid-like robot," in *2019 IEEE/RSJ International Conference on Intelligent Robots and Systems (IROS)*, pp. 5826–5831, IEEE, 2019.

[7] J. Frame, N. Lopez, O. Curet, and E. D. Engeberg, "Thrust force characterization of free-swimming soft robotic jellyfish," *Bioinspiration & biomimetics*, vol. 13, no. 6, p. 064001, 2018.

[8] C. Christianson, C. Bayag, G. Li, S. Jadhav, A. Giri, C. Agba, T. Li, and M. T. Tolley, "Jellyfish-inspired soft robot driven by fluid electrode dielectric organic robotic actuators," *Frontiers in Robotics and AI*, vol. 6, p. 126, 2019.

[9] Z. Ren, W. Hu, X. Dong, and M. Sitti, "Multi-functional soft-bodied jellyfish-like swimming," *Nature communications*, vol. 10, no. 1, pp. 1–12, 2019.

[10] J. Yu, J. Xiao, X. Li, and W. Wang, "Towards a miniature self-propelled jellyfish-like swimming robot," *International Journal of Advanced Robotic Systems*, vol. 13, no. 5, p. 1729881416666796, 2016.

[11] F. Berlinger, J. Dusek, M. Gauci, and R. Nagpal, "Robust maneuverability of a miniature, low-cost underwater robot using multiple fin actuation," *IEEE Robotics and Automation Letters*, vol. 3, no. 1, pp. 140–147, 2017.

[12] P. Hou, Z. Ye, and Z. Chen, "Bio-inspired robotic fish propelled by multiple artificial fins," in *ASME 2016 Dynamic Systems and Control Conference*, American Society of Mechanical Engineers Digital Collection, 2016.

[13] Y. Shan, Y. E. Bayiz, and B. Cheng, "Efficient thrust generation in robotic fish caudal fins using policy search," *IET Cyber-systems and Robotics*, vol. 1, no. 1, pp. 38–44, 2019.

[14] S. V. Patankar, *Numerical heat transfer and fluid flow*. Hemisphere Publishing Corporation, 1981.

[15] R. I. Issa, "Solution of the implicitly discretised fluid flow equations by operator-splitting," *Journal of Computational Physics*, vol. 62, pp. 40–65, Jan. 1986.

[16] T. Holzmann, *Mathematics, Numerics, Derivations and OpenFOAM®*. 12 2016.

[17] Z. Li, R. Mysa, R. Jaiman, and B. Khoo, "Freely vibrating circular cylinder in the vicinity of fully developed scour holes at low reynolds numbers," *Computers & Fluids*, vol. 163, pp. 97 – 120, 2018.

[18] R. C. Mysa and D. D. Chandar, "Edge curvature effects of a square cylinder on self-sustained oscillations," *Computers & Fluids*, vol. 170, pp. 273 – 284, 2018.

[19] R. G. Bottom II, I. Borazjani, E. L. Blevins, and G. V. Lauder, "Hydrodynamics of swimming in stingrays: numerical simulations and the role of the leading-edge vortex," *Journal of Fluid Mechanics*, vol. 788, pp. 407–443, 2016.

[20] R. C. Mysa and K. Venkatraman, "Intertwined vorticity and elastodynamics in flapping wing propulsion," *Journal of Fluid Mechanics*, vol. 787, pp. 175–223, 2016.